Journal of Neuroinflammation

RESEARCH Open Access

Targeting microglia-Th17 feed-forward loop to suppress autoimmune neuroinflammation

Jun Xiao[1,2], Zihan Meng[1], Yao Lu[1], Zongchang Nie[1], Yujie Liu[1], Zhi Yao[1*], Yingchi Zhang[2*] and Long Li[1*]

Abstract

Microglia and Th17 cells are the major immunopathogenic cells in multiple sclerosis and its animal model of immune aspects, experimental autoimmune encephalomyelitis (EAE). While studies have highlighted the distinct roles of microglia and Th17 cells in EAE, it remains unclear whether microglia, as potential professional antigen-presenting cells, activate and stabilize the effector program of EAE-pathogenic Th17 cells in vivo; and if so, whether the Th17 could in turn reinforce the active state of the microglia. Our data demonstrate in an array of mouse models, including active/passive-EAE and transgenic mice, a microglia-Th17 feed-forward activation loop drives EAE disease progression through a mechanism dependent on both MHC-II, proinflammatory cytokines, inflammatory chemokines as well as STING→NF-κB pathway in the microglia and effector cytokines produced by the pathogenic Th17 cells. We also captured and identified the molecular properties of the feed-forward loop, which are two-cell entities of microglia-Th17, and proved them as the functional units of antigen presentation and bi-directional activation between the two cell types. Moreover, ACT001, an orphan drug to treat glioblastoma, disrupts this feed-forward activation loop by inhibiting the STING→NF-κB pathway in microglia, thereby alleviating EAE. These findings emphasize the importance of interactions and bi-directional activations between microglia and Th17 in the autoimmune neuroinflammation, and provide rationale for further investigation on ACT001 as therapeutic option for autoimmune inflammatory diseases driven by similar mechanisms.

Keywords Microglia, Th17, Experimental autoimmune encephalomyelitis, ACT001

Introduction

Multiple sclerosis (MS) is a chronic disorder characterized by immune-mediated attacks to the myelin sheath of neurons, leading to demyelination, inflammation, and subsequent neurological dysfunction [1]. Experimental autoimmune encephalomyelitis (EAE) is an animal model that mimics key aspects of the immunopathogenesis in MS, including the activation and infiltration of $CD4^+$ T cells, particularly EAE-pathogenic autoimmune Th17 cells, into the central nervous system (CNS) [2–4].

The progression of EAE in mice is usually divided into two major phases: the induction phase and the effector phase (Fig. S1A) [3, 5]. In the induction phase, which covers from immunization of autoantigens, such as myelin oligodendrocyte glycoprotein (MOG) or myelin basic

*Correspondence:
Zhi Yao
yaozhi@tmu.edu.cn
Yingchi Zhang
zhangyingchi@ihcams.ac.cn
Long Li
Long.Li@tmu.edu.cn
[1]Tianjin Institute of Immunology, Key Laboratory of Immune Microenvironment and Disease (Ministry of Education), State Key Laboratory of Experimental Hematology, Department of Immunology, Tianjin Medical University, Tianjin 300070, China
[2]State Key Laboratory of Experimental Hematology, Haihe Laboratory of Cell Ecosystem, Institute of Hematology and Blood Diseases Hospital, National Clinical Research Center for Blood Diseases, Chinese Academy of Medical Sciences and Peking Union Medical College, Tianjin 300020, China

protein (MBP), to the time when the clinical signs start to be evident, the mice appear healthy; during this time, naïve $CD4^+$ T cells are primed by dendritic cells (DCs) in the peripheral lymphoid organs, leading to their differentiation into various Th cell subsets, including Th17 cells. During the effector phase of EAE, the mice show the typical clinical symptoms, such as paralysis, ataxia, and weight loss, and the primed Th17 cells migrate to the CNS, where they are activated by resident antigen-presenting cells (APCs), possibly DCs, microglia or monocytes, to developed into pathogenic Th17 cells that drive autoimmune inflammations [2, 6]. The two-phase process of EAE corresponds to a "two-step" priming-activation of Th17 cells: the initial prime in the lymph nodes followed by the activation within the CNS, paralleling the progression of EAE from immunization to disease onset, and then to peak severity [6, 7].

The "two-step" model of Th17 cell priming-activation has been recently experimentally validated, confirming that Th17 cells undergo initial priming in the lymph nodes before being restimulated and activated in the CNS [7]. Although this model provides a framework for studying Th17 cells in autoimmune inflammations, key questions remain regarding the mechanisms underlying the process, such as what triggers Th17 activation within the CNS of EAE/MS [8]. Microglia, the resident macrophages, are the most abundant immune cells in the CNS, and are thus potential APCs to trigger the activation of the primed Th17 cells [4, 9]. Furthermore, the activated EAE-pathogenic Th17 cells produce GM-CSF and IFNγ, the cytokines that may in turn activate the microglia from homeostatic state. Therefore, we hypothesized that microglia and Th17 interact with each other and form a feed-forward activation loop that maintains and reinforces both the effector program of pathogenic Th17 cells and the active state of microglia in the lesions of EAE mice.

ACT001, an orphan drug approved by the US FDA to treat glioblastomas [10], is derived from micheliolide (MCL) [11], a natural compound with known anti-inflammatory functions [12]. ACT001 has several properties making it a promising medicine for treating neuroinflammation, including its ability to cross the blood-brain barrier [13, 14], low systemic and local toxicity [10, 15], and its ability to alleviate traumatic brain injury-related neuroinflammation [16]. Despite these favorable attributes, its efficacy in mitigating the autoimmune inflammation in EAE has not yet been explored, and deserves further investigation to provide a foundation for its possible role in treating MS.

In this report, we tested the hypothesis that the interactions between Th17 and microglia stabilized the activation of both cells in EAE, and investigated the efficacy and mechanism by which ACT001 treated EAE. The findings demonstrate a feed-forward activation loop between microglia and Th17 cells at the lesions of EAE. The loop is critically mediated by MHC-II, proinflammatory cytokines and chemokines from microglia, and by IFNγ and GM-CSF from the pathogenic Th17 cells. The STING→NF-κB signaling pathway in microglia fueled the elevated expression of the above-mentioned genes in microglia and thus stabilizes the activate state of the cells, which fueled the feed-forward activation loop and exacerbated the autoimmune neuroinflammation. ACT001 effectively suppressed the STING→NF-κB pathway in microglia, thus disrupted the feed-forward activation loop and resulted in much milder EAE, suggesting its potential as a therapeutic agent for autoimmune neuroinflammatory diseases like multiple sclerosis.

Materials and methods

Mouse strains

C57BL/6J, *Sting1*$^{-/-}$ and 2D2 mice were bred and housed under specific-pathogen-free (SPF) conditions, with controlled temperature (21–23 °C), humidity (30–70%), and a 12-hour light/dark cycle, in the animal facility at Tianjin Medical University. All experimental procedures involving age-matched (8-week young at immunization of MOG_{35-55}) female mice were conducted in accordance with protocols approved by the Institutional Animal Care and Use Committee of Tianjin Medical University.

Induction of EAE and administration of ACT001

The mice were immunized subcutaneously with 200 μg of MOG_{35-55} peptide (MEVGWYRSPFSRVVHLYRNGK) emulsified in complete Freund's adjuvant (CFA) containing 5 mg/ml non-viable *Mycobacterium tuberculosis* H37Ra. Additionally, pertussis toxin (200 ng) in PBS were administered i.p. followed on the day of immunization and 48 h later. After the immunization, neurological defects were assessed according to the clinical syndromes in the mice, which were scored using the following scoring system: 0, no obvious changes in motor functions; 1.0, limp tail; 2.0, limp tail and wobbly gait; 3.0, bilateral hind limb paralysis; 4.0, front and hind limb paralysis; and 5.0, moribund state [17–19]. The EAE model in the study is chronic; therefore, the disease progression of EAE is defined as the continuous increase in EAE clinical scores from onset to the peak of clinical signs. ACT001 (100 mg/kg of bodyweight in saline) or saline was administered by gavage.

Flow cytometry

To isolate mononuclear cells from spinal cords during EAE, spinal cords were mechanically disrupted and dissociated in ice-cold RPMI-1640 using a Dounce homogenizer. Tissue cells were resuspended in 30% working isotonic Percoll (WIP) to a final volume of 5 ml. The cell

suspension was then layered on top of 10 ml of 70% WIP, ensuring the formation of a distinct flat interface at the 70%-30% junction. The gradient was centrifuged at 500 × g for 20 min at 20℃, with the centrifuge set to stop with minimal or no braking to avoid disturbing the interphase. Leukocytes were collected from the interface of the 30%/70% WIP gradient and washed twice with FACS buffer.

Single cell suspensions were pelleted and resuspended in FACS buffer containing anti-CD16/anti-CD32, along with surface-staining antibodies. Surface staining was performed for 20–30 min on ice. Subsequently the cells were washed and resuspended in Zombie NIR™ Fixable Viability dye for 15 min prior to fixation. For intracellular staining, lymphocytes were cultured in RPMI-1640 medium containing 10% fetal bovine serum (FBS), 1% penicillin-streptomycin, and 55 μM of β-mercaptoethanol, and stimulated for 6 h with Cell Activation Cocktail with Brefeldin A. Following surface and viability staining, intracellular cytokine staining was performed using Cyto-Fast™ Fix/Perm Buffer Set, and transcriptional factor staining was carried out using the True-Nuclear™ Transcription Factor Buffer Set, following the manufacturer's protocol. Stained cells were analyzed on FACS Canto II flow cytometer using FACSDiva software, and data were further analyzed with FlowJo software.

In vitro T cell activation, differentiation and proliferation

Lymphocytes were isolated from spleens and peripheral lymph nodes of wide-type C57BL/6 mice. Total $CD4^+$ T cells were enriched using the CD4 T Cell Isolation Kit (Negative selection), followed by stained with Zombie NIR™ Fixable Viability dye, PE-Cy7 Anti-CD4, FITC Anti-CD44 and Percp-Cy5.5 Anti-CD62L antibodies for FACS sorting using FACS arial II. Purified $CD4^+CD62L^+CD44^-$ naïve $CD4^+$ T cells were then plated at a density of 1×10^5 cells per well and cultured in RPMI-1640 medium containing 10% FBS, 1% penicillin-streptomycin and 55 μM of β-mercaptoethanol. Cells were activated with plate-coated anti-CD3 (2.5 μg/ml) and anti-CD28 (2.5 μg/ml) antibodies.

For Treg cell differentiation, rhTGF-β1 (5 ng/ml) and rmIL-2 (5 ng/ml) were added to the culture medium. For Th1 differentiation, rmIL-12 (20 ng/ml) and anti-mIL-4 (20 μg/ml) were included. For Th17 differentiation, rmIL-6 (20 ng/ml), rhTGF-β1, rmIL-1β (20 ng/ml), rmIL-23 (50 ng/ml), anti-mIFNγ (5 μg/ml), and anti-mIL-4 (5 μg/ml) were added to the culture.

Adoptive transfer of $CD4^+$ T cells

Lymphocytes were isolated from the draining lymph nodes of donor mice. Total $CD4^+$ T cells were enriched using a $CD4^+$ T Cell Isolation Kit (negative selection). The enriched $CD4^+$ T cells were administered to recipient mice (5×10^6 cells per mouse) via retro-orbital injection.

Histopathology

For the assessment of tissue pathology, spinal cords were removed, washed twice with PBS, and fixed in 4% paraformaldehyde for 48 h. The tissues were processed and embedded in paraffin wax. For haematoxylin and eosin (H&E) staining, transverse sections of the lumbar spinal cord were deparaffinized and rehydrated using standard procedures, followed by staining with H&E staining. Spinal cord sections were selected from the same anatomical region for consistent lateral comparison. The "infiltration area" was calculated as the combined area of immune cell infiltration and demyelination by ImageJ. The data were then normalized to the samples from control mice to generate the "Relative infiltration area" for standardized comparison across experimental groups.

For immunofluorescence staining, transverse sections of the lumbar spinal cord were deparaffinized and rehydrated using standard procedures. The sections underwent antigen retrieval with sodium citrate antigen retrieval solution at 98 °C for 20 min, followed by natural cooling to room temperature. Sections were then incubated in TBS containing 0.25% Triton X-100 for 10 min, and subsequently blocked in 10% goat serum with 1% BSA in TBS for 2 h at room temperature to prevent secondary antibody cross-reactions with endogenous immunoglobulins. The primary antibody, diluted in TBS with 1% BSA, was applied and incubated overnight at 4 °C. After washing five times with TBS, a fluorophore-conjugated secondary antibody was applied to the slides and incubated for 1 h at room temperature, followed by five washes with TBS. The sections were then mounted using a mounting medium containing DAPI, and a coverslip was added.

Preparation of microglia for in vitro culture

Cerebral cortices from neonatal mice (within 24 h after birth) were collected, and the meninges and blood vessels were carefully removed. Following dissection, the tissues were digested with 0.25% trypsin-EDTA and washed with Hank's Balanced Salt Solution (HBSS) containing FBS. Single-cell suspensions were obtained by passing the tissues through a 70 μm cell strainer. The cells were seeded into poly-D-lysine-precoated flasks and cultured in DMEM/F12 medium supplemented with 10% FBS at 37 °C in 5% CO_2. The culture medium was replaced every 4 days. After 12 days, microglia were separated from the underlying astrocytic layer by gentle shaking of the flask and were plated overnight in poly-D-lysine-precoated plates.

Immunoblotting

Cells were washed with PBS buffer and lysed in cold lysis buffer (50 mM HEPES, pH 7.4, 150 mM NaCl, 1% (v/v) NP-40) supplemented with a protease inhibitor cocktail. The lysate was clarified by centrifugation at 13,600 × g at 4 °C. The resulting supernatant was boiled in 5× loading buffer for SDS–polyacrylamide gel electrophoresis (SDS-PAGE), followed by transfer to polyvinylidene difluoride (PVDF) membranes (0.45 μm). The membranes were blocked for 1 h using 5% bovine serum albumin (BSA) with 0.1% Tween 20 in TBST buffer. After blocking, the membranes were washed and incubated overnight with primary antibodies at 4 °C. Secondary antibodies, either goat anti-rabbit or goat anti-mouse IgG (1:5000 dilution), were applied for 1 h at room temperature. Finally, after additional washes, immunoreactive bands were visualized using enhanced chemiluminescence (ECL) and developed using a Western blot imaging system. Quantification of the Western blot images was performed using ImageJ to calculate the darkness of the bands.

RNA Preparation and quantitative PCR

Total RNA was extracted from cells using TRIzol reagent according to the manufacturer's protocol and reverse-transcribed into complementary DNA (cDNA) using the TransScript cDNA Synthesis Kit. Quantitative PCR (qPCR) was performed using the LightCycler® 96 system instrument with specific primers. Reactions were carried out using SYBR Green, and relative gene expression levels were calculated by the ΔΔCt method, normalized to a housekeeping gene.

RNA-seq

For RNA sequencing (RNA-seq) analysis, total RNA was extracted from sorted single live Tmem119$^+$ cells in CNS lesions using TRIzol reagent. RNA enrichment was performed using Oligo(dT) magnetic beads, and the enriched RNA was used for constructing BGISEQ-500 libraries. The RNA-seq libraries were sequenced using the BGISEQ-500 platform, following the 50 bp single-end protocol as per the manufacturer's instructions. After sequencing, adaptors and low-quality reads were removed to obtain clean reads, ensuring each sample contained more than 26 million reads. The clean reads were mapped to the mouse reference genome using HISAT2/Bowtie2, and the mapping results were stored as BAM files using SAMtools. Total read counts at the gene level were summarized using the featureCounts function from the Rsubread package, while gene and transcript annotation was performed with the biomaRt R package.

Differential gene expression analysis was conducted using the DESeq2 package with default settings, with total read counts as the input. Genes with an adjusted p-value (padj) < 0.05 were considered differentially expressed. Heat maps of gene expression were generated using z-score values from the normalized expression matrix obtained from DESeq2 and visualized using SRplot (https://www.bioinformatics.com.cn/srplot).

Statistical analysis

All statistical analyses and plotting were performed using GraphPad Prism 8. Statistical significance was determined using either a two-tailed Student's *t*-test, one-way ANOVA, or two-way ANOVA with Tukey's post-hoc correction, as specified in the figure legends. Error bars represent the mean ± SEM of biological triplicates. P-values are indicated as follows: n.s. (not significant), or with asterisks to denote levels of significance ($^*p < 0.05$; $^{**}p < 0.01$; $^{***}p < 0.001$; $^{****}p < 0.0001$).

Results

ACT001 ameliorates EAE at the effector phase of the disease

To determine whether ACT001 had therapeutic effects on EAE and to identify the specific phase during which it might exert the effects, ACT001 was administered to EAE mice on following regime: a control group without ACT001 (EAE-control) treatment, an induction-effector (I-E) group receiving ACT001 during both the induction and effector phases of EAE, and two additional groups receiving the treatment either during the induction phase or during the effector phase, respectively (Fig. 1A and Fig. S1A). The results showed that ACT001 had no therapeutic effect when administered only during the induction phase (induction-only group). However, ACT001 significantly reduced the severity of the symptoms of EAE in both I-E and effector-only groups (Fig. 1B, C and Fig. S1B, C). Histopathological analysis showed significant demyelination as well as infiltration of immune cells in the spinal cord (SC) sections of EAE-control and induction-only groups, whereas the samples from I-E and effector-only groups had much less infiltration of immune cells and no obvious demyelination (Fig. 1D, E, and Fig. S1D). Flow cytometry analysis confirmed that the numbers of SCs-infiltrating CD45$^+$ immune cells and CD4$^+$ T cells in the I-E and effector-only groups where ACT001 treatment was effective were much less than those in induction-only as well as the EAE-control groups (Fig. 1F, G). Additionally, the isolated CD45$^+$ infiltrating cells from the SCs in the groups with effective ACT001 treatment expressed less inflammatory cytokines associated with severity of EAE, including *Il1b*, *Csf2*, *Il6*, *Il17a* and *Ifng*, whereas these cells expressed high levels of anti-inflammatory cytokine *Il10* (Fig. 1H).

Comprehensively, the results revealed that ACT001 ameliorated EAE at the effector phase of the disease without affecting the onset of clinical symptoms, and furthermore, treatment during the effector phase was sufficient

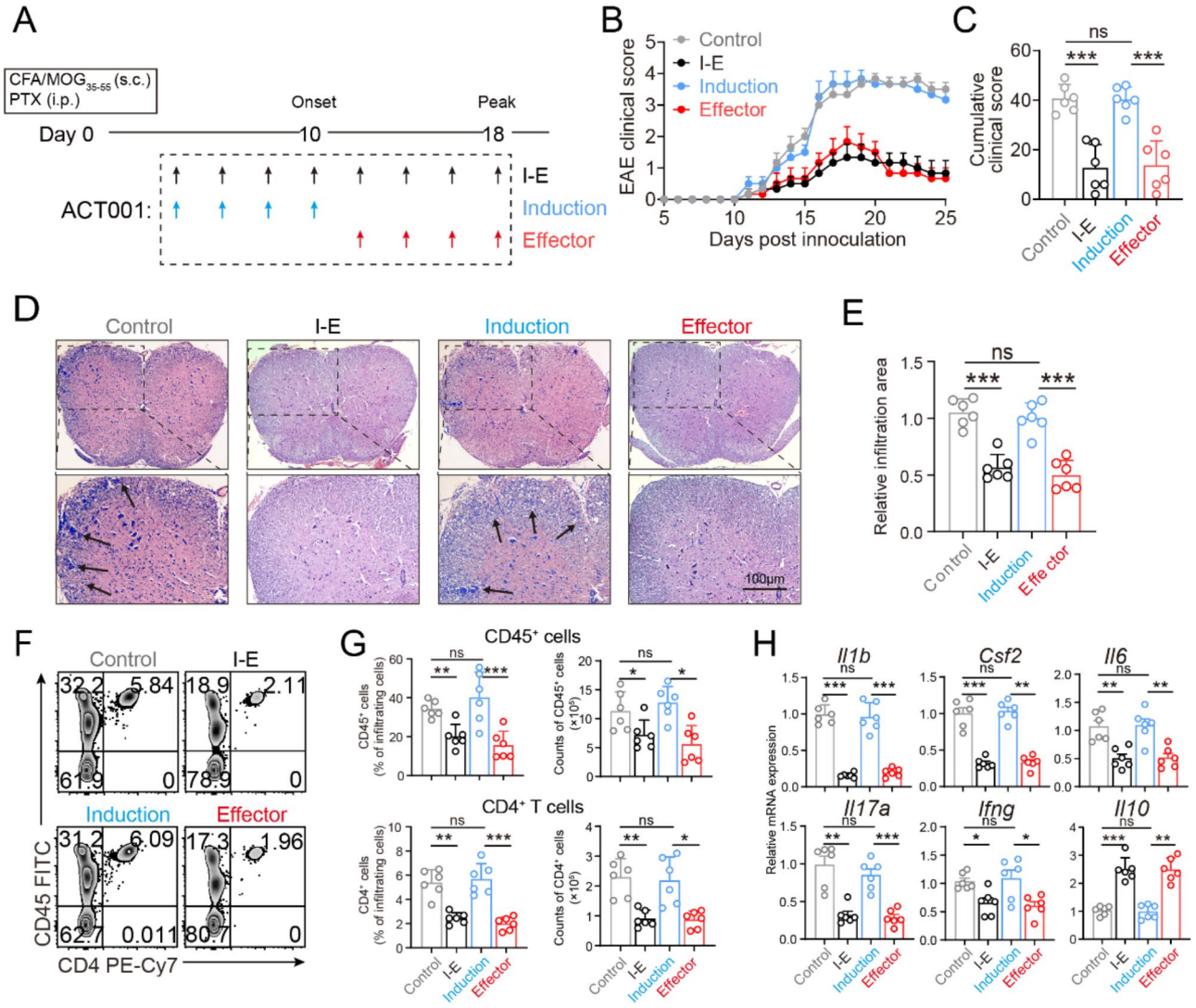

Fig. 1 ACT001 alleviates autoimmune-mediated neuroinflammations. **(A-C)** Severity of EAE in the C57BL/6 mice subjected to different time-point treatments with ACT001 ($n=6$ per group). **(A)** Schematic representation of EAE induction and ACT001 treatments. Following EAE induction, the mice were randomly allocated into four groups: the Control group (no treatment), the I-E group (treatment during both induction and effector phases), the Induction group (treatment during the induction phase only), and the Effector group (treatment during the effector phase only). **(B)** Mean daily disease score of the mice. **(C)** Cumulative clinical score of the mice. **(D-G)** Infiltrations of inflammatory cells in the SCs ($n=6$ per group). **(D)** Representative H&E staining images. **(E)** Quantitative analysis of areas of infiltrations of inflammatory cells in transverse sections of the SCs. **(F)** Representative flow cytometry analysis of SCs-infiltrating $CD45^+$ cells and $CD4^+$ T cells. **(G)** Statistical analysis of the frequencies and absolute numbers of $CD45^+$ cells and $CD4^+$ T cells in **(F)**. **(H)** Normalized mRNA expressions of EAE-related cytokines in SCs-infiltrating $CD45^+$ cells. Statistics were calculated using one-way ANOVA with Tukey's correction. Error bars represent the mean ± SEM with ns indicating not significant, $^*p<0.05$, $^{**}p<0.01$, and $^{***}p<0.001$

and necessary for its therapeutic effects. Therefore, we decided to further investigate the mechanisms underlying the therapeutic effects of ACT001 on EAE.

ACT001 destabilizes the effector program of pathogenic Th17 in the lesions of EAE

To study the mechanisms by which ACT001 ameliorated EAE during the effector phase, we conducted experiments with ACT001 administered exclusively during the effector phase (Fig. S2A). Given that the major sublineages of $CD4^+$ T cell involved in EAE/MS pathogenesis include the pro-inflammatory Th1 and Th17 cells, which act as positive contributors, and Treg cells, which may suppress the inflammation, this part of research aimed to determine the specific lineage and

the functional states of CD4⁺ T cells that were targets of ACT001 during the effector phase of EAE [20, 21] (Fig. S2B).

We first assessed the number of total CD4⁺ T cells in inguinal lymph nodes (iLNs) and SCs at the peak of EAE clinical signs, and found that ACT001 did not alter the number of total CD4⁺ T cells in iLNs, but the number of total CD4⁺ T cells in the SCs decreased significantly compared to the control group (Fig. 2A, B). We next analyzed the specific CD4⁺ T cell lineages individually. As for Foxp3⁺ Treg, there was no significant change in the proportions or numbers of these cells (Fig. 2C, D) between the ACT001-treated EAE-mice and the EAE-controls in either iLNs or SCs. We then analyzed CD4⁺ T cells based on their expressions of effectors IFNγ, IL-17 A and GM-CSF. The results showed that the proportions and numbers of Th1 cells (IFNγ⁺IL17A⁻, highlighted by green in Fig. 2E, F) and IFNγ⁻ Th17 cells (IFNγ⁻IL17A⁺, highlighted by yellow in Fig. 2E, G) in the iLNs were not affected by ACT001. However, in the

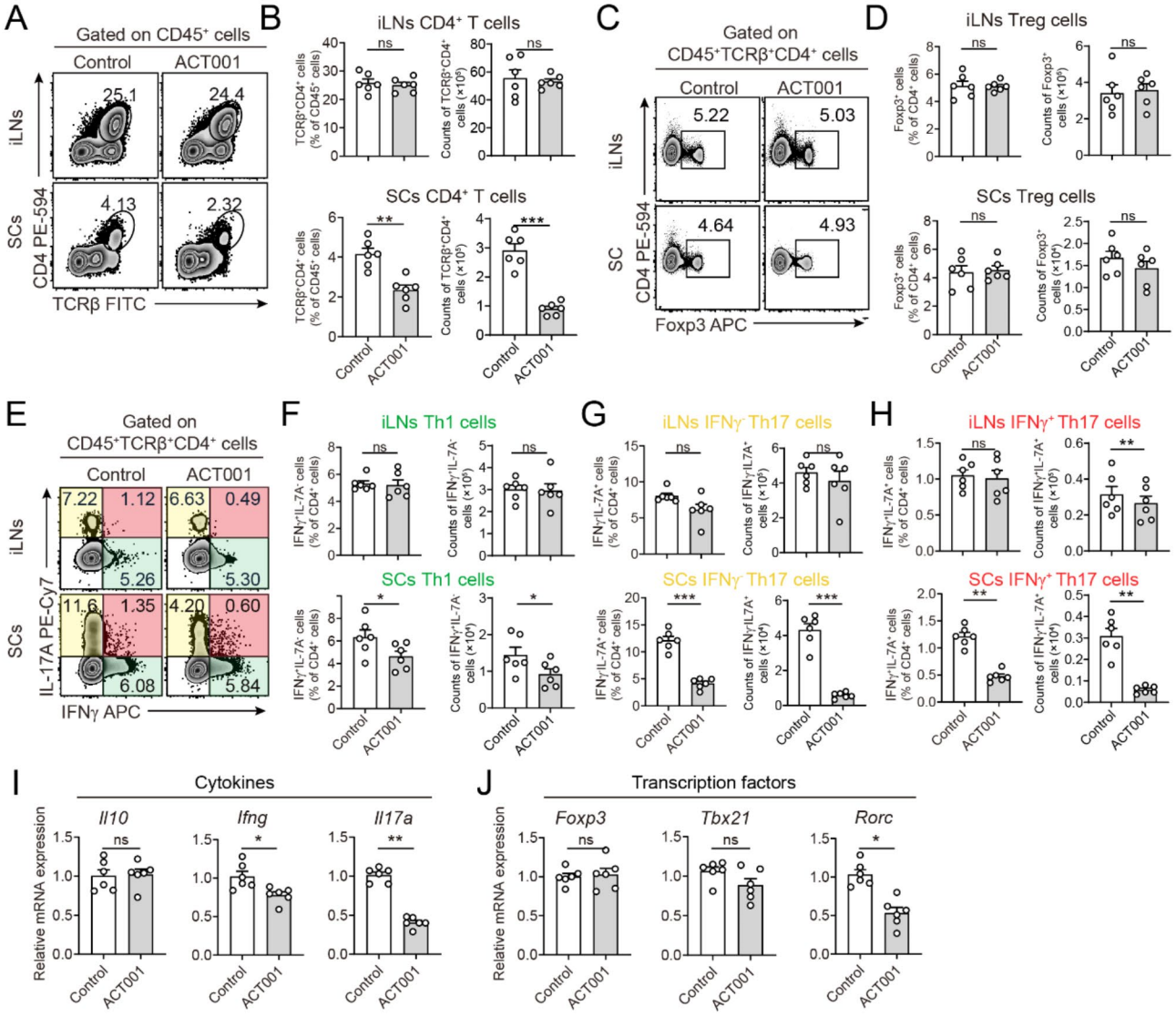

Fig. 2 ACT001 dampens the effector program of Th17 in the spinal cords of EAE mice. **(A-B)** Flow cytometry analysis of CD4⁺ T cells in iLNs and SCs was performed at the peak of EAE ($n = 6$ per group). **(A)** Representative flow cytometry results of CD4⁺ T cell gated on CD45⁺ cells. **(B)** Statistical analysis of the frequencies and absolute numbers of CD4⁺ T cells in **(A)**. **(C-D)** Flow cytometry analysis of Treg cells in iLNs and SCs at the peak of EAE. **(C)** Representative flow cytometry results of CD4⁺Foxp3⁺ Treg cells. **(D)** Statistical analysis of the frequencies and absolute numbers of Treg cells in **(C)**. **(E-H)** Flow cytometry analysis of Th1 and Th17 cells in iLNs and SCs at the peak of EAE. Representative flow cytometry results are shown in **(E)**, along with statistical analysis of the frequency and absolute numbers of Th1 **(F)**, IFNγ⁻ Th17 **(G)**, and IFNγ⁺ Th17 **(H)** cells. **(I-J)** Normalized mRNA expressions of cytokines **(I)** and transcription factors **(J)** associated with Treg, Th1 and Th17 in CD4⁺ T cells isolated from SCs at the peak of EAE. Statistics were calculated using the unpaired sample *t*-test. Error bars represent the mean ± SEM, with ns indicating not significant, $*p < 0.05$, and $**p < 0.01$

SCs, the proportions and numbers of IFNγ$^-$ Th17 cells (Fig. 2E, G) and IFNγ$^+$ Th17 cells (IFNγ$^+$IL17A$^+$, highlighted by red in Fig. 2E, H) were significantly reduced by ACT001 treatment. Furthermore, the proportion and number of GM-CSF$^+$ Th17 cells, which are thought to be closely associated with the severity of EAE and may participate in interactions with antigen-presenting cells [4, 22–25], reduced significantly in the SCs by ACT001 during the EAE effector phase (Fig. S2C, D). The cellular changes suggested that Th17, especially the EAE-pathogenic GM-CSF$^+$ Th17 in the SCs lesions, might be the targets of ACT001 at the effector phase of EAE. The mRNA expression of characteristic genes associated with Th1, Th17 and Treg in sorted CD4$^+$ T cells from the SCs lesions supported this notion, as well, for that the expressions of *Ifng*, *Il17a* and *Rorc*, all of which are related to the effector program of Th17, were significantly reduced by ACT001, whereas ACT001 had little effect on the genes associated with the effector programs of Treg or Th1 (Fig. 2I, J) [7, 24, 25].

Our results showed that ACT001 did not affect the proportions or numbers of Treg, Th1, or Th17 cells in iLNs, suggesting that ACT001 did not target T cells in the priming phase. However, ACT001 markedly reduced the expression of effector genes as well as the proportion and number of Th17 cells in the SCs, which prompted us to propose that ACT001 affected Th17 during the activation phase in the SCs, consistent with its therapeutic effects observed during the effector phase of EAE (Fig. 1B, C). Therefore, we decided to focus on the activation of Th17 in the SCs (the effector phase of EAE) to study the mechanisms by which ACT001 ameliorates EAE.

The therapeutic effects of ACT001 are associated with the activation phase of Th17 cells rather than their priming phase

To prove our hypothesis and to determine how ACT001 inhibited the effector program of Th17, we performed adoptive transfer of CD4$^+$ T cell in mice [26, 27] to pinpoint the specific phase during which ACT001 suppressed the Th17 effector program. In the EAE model, the induction phase corresponds to the initial priming of Th17 in iLNs, while the effector phase is related to the activation of Th17 in the lesion foci (Fig. S1A) [2, 6, 7, 25]. This theory was incorporated into the experiment design. EAE was first induced in the donor mice, and on day 10, right before the EAE-clinical signs showed up, CD4$^+$ T cells were isolated from iLNs and expanded in vitro. The polarization of these cells, both in vivo and in vitro, simulated the priming phase of Th17 cells. These expanded CD4$^+$ T cells were then transferred into the recipient mice, where they induced EAE, thereby simulating the activation process (Fig. 3A, G) [7, 25]. This approach enabled us to clearly distinguish the effects of ACT001 on Th17 between the priming and activation phases in vivo. The results showed that ACT001 administered during the priming phase did not significantly alter the capacity of CD4$^+$ T cells to induce EAE in the recipient mice (Fig. 3A), as EAE clinical scores (Fig. 3B), infiltration of inflammatory cells (Fig. 3C) and Th17 cell effector function (Fig. 3D-F) revealed no suppression of the Th17 effector program by ACT001 during priming phase. However, when administered only during the activation phase of Th17 in the recipient mice (Fig. 3G), ACT001 proved effective, with the treated mice exhibiting significantly lower clinical scores (Fig. 3H), reduced infiltration of inflammatory cells (Fig. 3I) and diminished Th17 effector function (Fig. 3J-L) compared to the control mice. These findings confirmed that ACT001 primarily exerted its therapeutic effects during the activation phase of Th17, which corresponds to the effector stage of EAE. To further validate this, we sorted naïve CD4$^+$ T cells and conducted in vitro experiments to evaluate whether ACT001 affected the differentiation of CD4$^+$ T cell lineages (Fig. S3A) [24, 25, 28, 29]. The results showed that ACT001 did not alter the differentiation of Th17 (Fig. S3B-D), Th1 (Fig. S3E-G) or Treg (Fig. S3H-J). Apparently, the fact that ACT001 has no significant effect on the differentiation of Th17 in vitro was contradictory to its strong inhibitory effects on the activation phase of Th17 in vivo. This led us to speculate that Th17 cells were not the direct target of ACT001 in EAE, and ACT001 might exert its therapeutic effects by modulating the cells that interact with Th17 in the EAE lesions.

ACT001 exerts therapeutic effects in EAE by inhibiting the activation of microglia

The activation phase of Th17 within the CNS relies on specialized antigen-presenting cells [4, 9, 21, 30]. Microglia, the resident macrophages and the most abundant immune cells in the CNS, are the most possible antigen-presenting cells in EAE lesions [4, 31, 32], although their role in antigen presentation and the activation of Th17 in the CNS remains unclear [4, 33–35]. Therefore, we aimed to confirm the role of microglia in the activation of Th17 in EAE and to determine whether ACT001 regulated this process. To determine whether ACT001 alters the functional state of microglia, we first assessed the number of microglia and their effector function in the SCs at the peak of EAE (Fig. S4A). The results showed that ACT001 treatment during the EAE-effector phase led to a reduction in the proportion of CD45^{Hi}CD11b$^+$ active microglia and an increase in the proportion of CD45^{dim}CD11b$^+$ homeostatic microglia (Fig. 4A, B and Fig. S5A, B) [32, 33]. In this study, "active" microglia is characterized by high expressions of *Nos2*, *Il1b* and *Tnf*, but low expressions of *Mcr1* and *Il10*, indicating a pro-inflammatory state. "Homeostatic" microglia refers to the

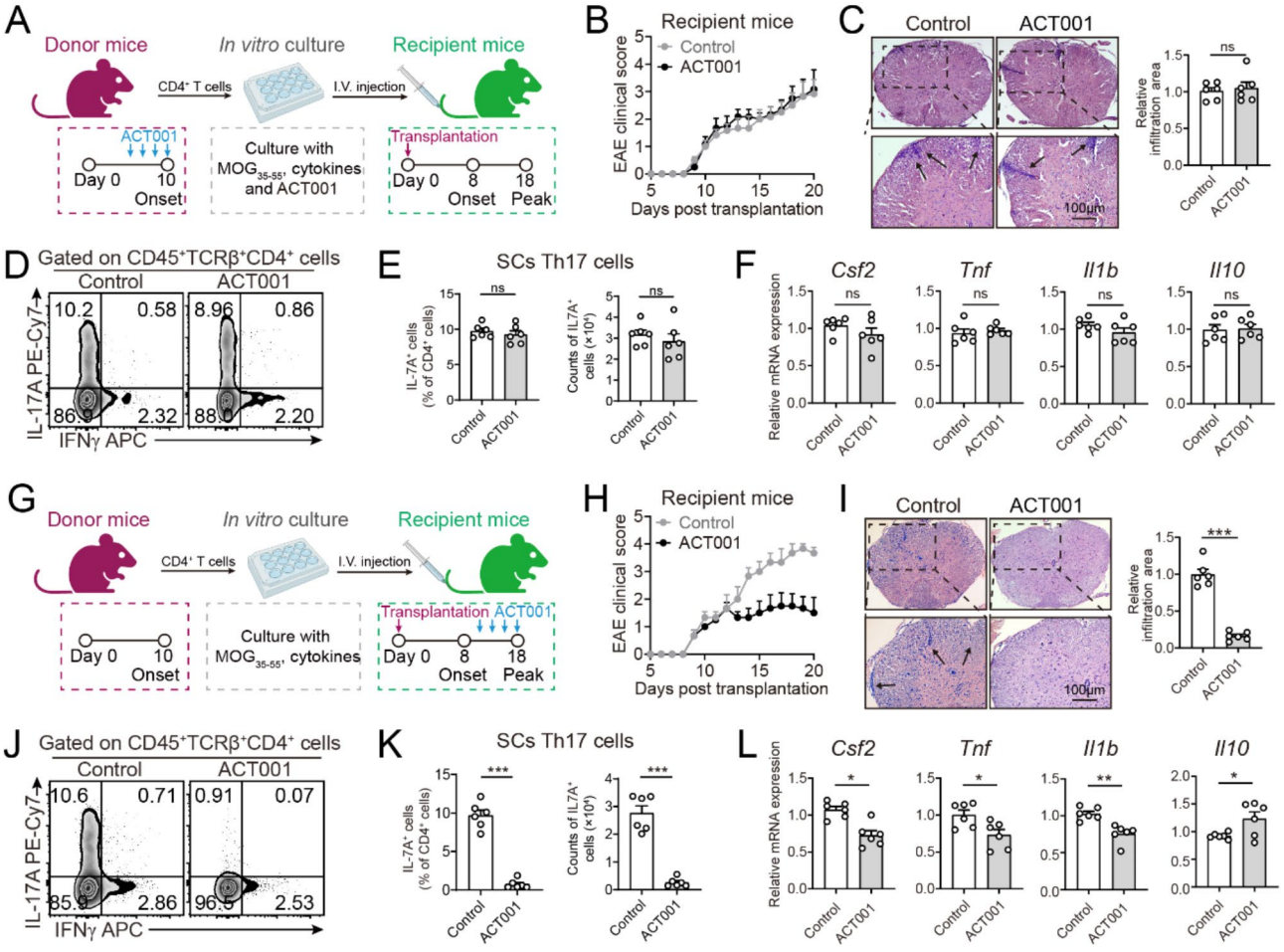

Fig. 3 ACT001 inhibits the activation of Th17 in the CNS during the effector phase of EAE. **(A)** Experimental schemes to investigate the possible role of the ACT001 in the priming phase of Th17 cells. EAE model was established in the donor mice. On day 10 (Onset), $CD4^+$ T cells from donor iLNs were isolated and cultured in vitro. ACT001 was administered during both in vivo treatment of donor mice and in vitro expansion of $CD4^+$ T cells. The expanded cells were then transplanted into recipient mice to assess the Th17 activation and the severity of EAE ($n=6$ per recipient group). **(B-C)** EAE severity of recipient mice in **(A)**. **(B)** Mean daily disease score of recipient mice. **(C)** Representative H&E staining images and quantitative analysis of inflammatory cell infiltration areas in the SCs. **(D-E)** Representative flow cytometry analysis **(D)** and statistical analysis of the frequencies and absolute numbers **(E)** of SCs-infiltrating Th17 cells in recipient mice at day 18 post-transplantation. **(F)** Normalized mRNA expressions of EAE-related cytokines in SCs. **(G)** Experimental schemes to investigate the role of ACT001 in the activation phase of T cells. In vivo modeling and in vitro expansion were conducted as described in **(A)**. ACT001 was administered only during the EAE effector phase in recipient mice ($n=6$ per recipient mice group). **(H-I)** EAE severity of the recipient mice in **(G)**. **(H)** Mean daily disease score of recipient mice. **(I)** Representative H&E staining images and quantitative analysis of inflammatory cell infiltration areas in the SCs. **(J-K)** Representative flow cytometry analysis **(J)** and statistical analysis of the frequencies and absolute numbers **(K)** of SCs-infiltrating Th17 cells in recipient mice at day 18 post-transplantation. **(L)** Normalized mRNA expressions of EAE-related cytokines in SCs. Statistics were calculated using the unpaired sample *t*-test. Error bars denote the mean ± SEM, ns = not significant, $*p<0.05$, $**p<0.01$ and $***p<0.001$

cell in a baseline, immunologically regulated state associated with immune regulation rather than inflammation, which is characterized by the expression of *Mcr1* and *Il10* [36]. Further analysis showed that ACT001 treatment led to reduced expression of major histocompatibility complex class II (MHC-II) (Fig. 4C, D) and iNOS (Fig. S5C, D) compared to the control group. The protein level of CD206, a marker of homeostatic microglia, was higher in the ACT001-treated group (Fig. S5E, F) [31, 33]. Additionally, ACT001 significantly downregulated mRNA expression of *Nos2*, *Il1b* and *Tnf*, effectors associated with active microglia (Fig. S5G), while the mRNA expressions of genes associated with homeostatic microglia (Fig. S5H), such as *Mrc1*, *Il4* and *Il10*, were significantly higher in the isolated microglia from the mice in ACT001-treated group. The data collectively revealed that ACT001 effectively shifts the functional state of microglia in the EAE lesions in vivo from active to homeostatic state. The fact that MHC-II was reduced in microglia from the EAE mice receiving ACT001 was especially interesting for that it suggested

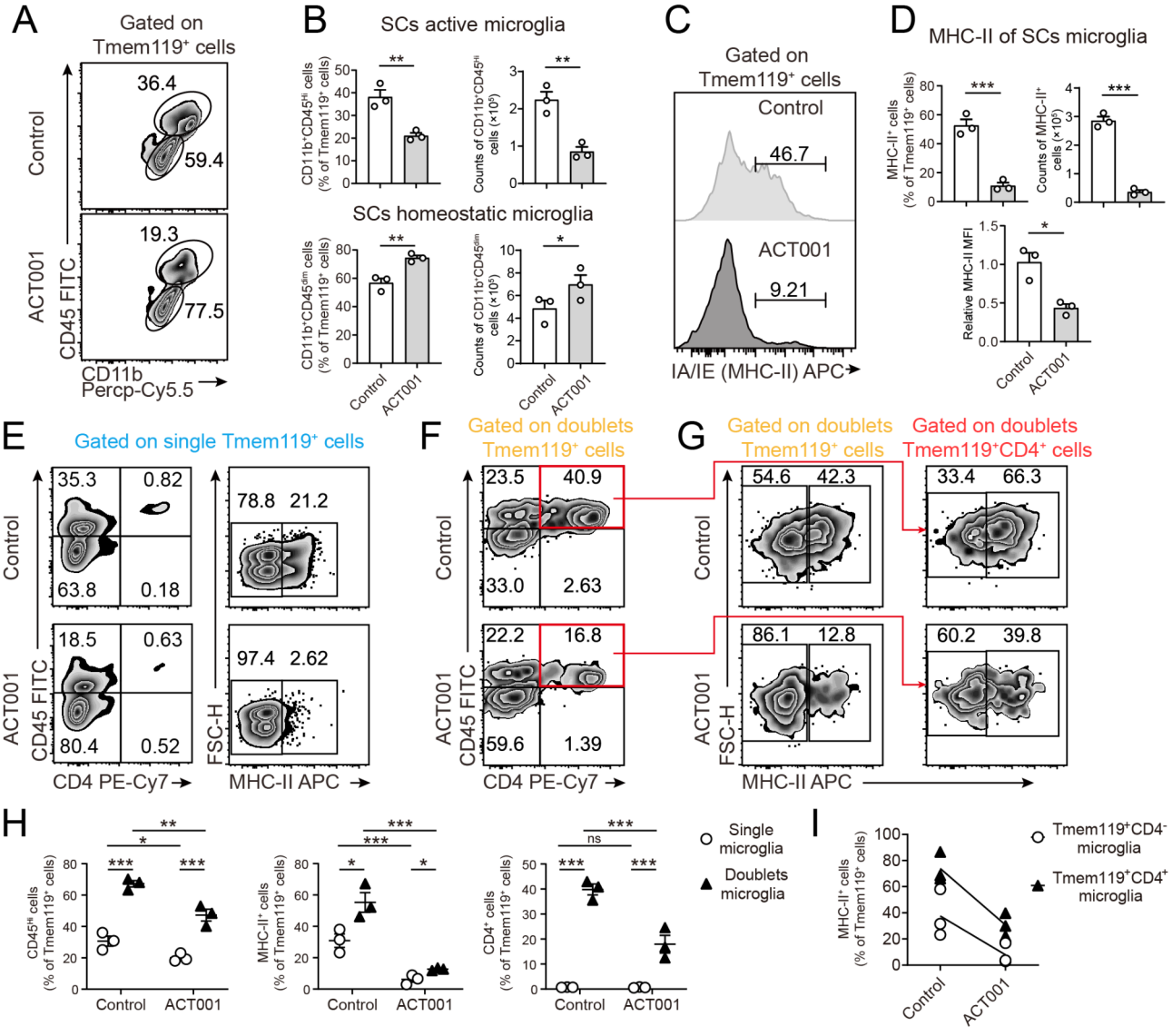

Fig. 4 ACT001 maintains microglial homeostasis and dampens their interactions with CD4⁺ T cells in vivo. **(A-B)** Flow cytometry analysis of active and homeostatic microglia in the SCs was performed at the peak of EAE, comparing ACT001-treated mice to controls ($n = 3$ per group). **(A)** Representative flow cytometry results of CD11b⁺CD45^{Hi} active microglia and CD11b⁺CD45^{dim} homeostatic microglia gated on Tmem119⁺. **(B)** Statistical analysis of the frequencies and absolute numbers of the microglia in **(A)**. **(C-D)** Flow cytometry analysis of IA/IE (MHC-II) expression on microglia. **(C)** Representative flow cytometry results of MHC-II expression gated on Tmem119⁺ microglia. **(D)** Statistical analysis of the frequencies, absolute numbers, and mean fluorescence intensity (MFI) of MHC-II expression on microglia in **(C)**. **(E-F)** Flow cytometry analysis of the interactions between Tmem119⁺ microglia and CD4⁺ T cells in single-cell **(E)** or doublet states **(F)**, as well as the effect of ACT001 on this interaction. The Tmem119⁺CD4⁺ gate indicates the interacting microglia and CD4⁺ T cells. **(G)** Flow cytometry analysis of MHC-II expression by microglia in the doublets. The colors of the subtitles of (E-G) correspond to the colors in the gating strategy shown in Fig. S4C. **(H)** The frequencies of CD45^{Hi} microglia, MHC-II⁺ microglia, and CD4⁺ T cell-interacting microglia in single-cell or doublet states were statistically analyzed, along with the effects of ACT001. **(I)** Comparisons of the expression of MHC-II in Tmem119⁺CD4⁺ microglia and Tmem119⁺CD4⁻ microglia, as well as the effects of ACT001. Statistics were calculated using the unpaired sample *t*-test **(B, D)** and two-way ANOVA with Tukey's correction **(H)**. Error bars denote the mean ± SEM, ns = not significant, $^{*}p < 0.05$, $^{**}p < 0.01$ and $^{***}p < 0.001$

antigen presentation by microglia was a possible target of ACT001, as well. Therefore, we focused our next efforts on this.

We categorized the interaction states of microglia and CD4⁺ T cells in the SCs into three distinct populations: individual microglia, individual CD4⁺ T cells, and interacting microglia-CD4⁺ T cell doublets based on Tmem119 and CD4, as well as forward scatter area (FSC-A) and forward scatter height (FSC-H) (Fig. S4B) [34]. In this analytic schema, the cellular entity with both CD4 and Tmem119 on the surface were interacting microglia and CD4⁺ T cell (Fig. S4C, analytic schema shown in orange box), which are the cells engaged in antigen presentation. The results showed that the single-cell

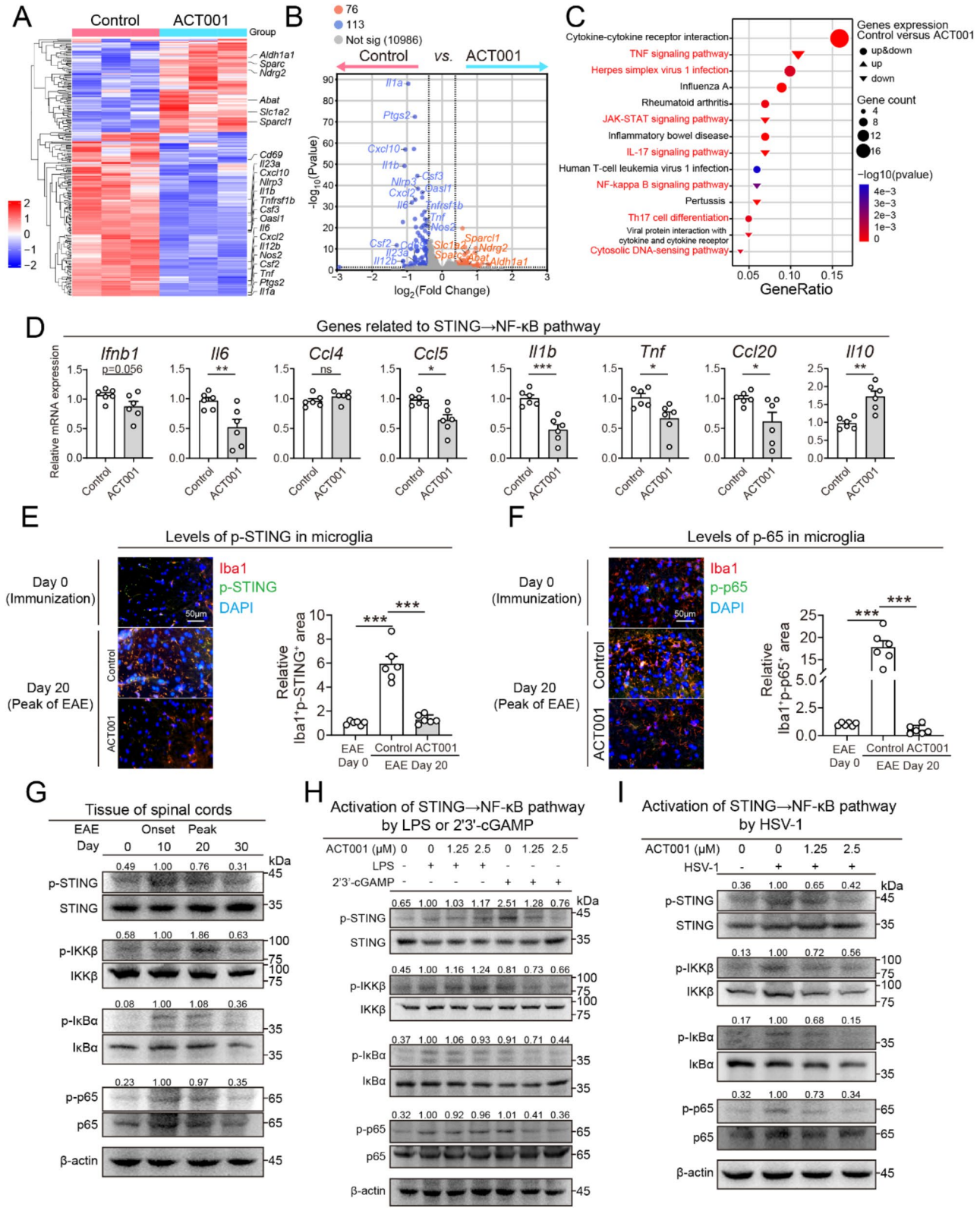

Fig. 5 (See legend on next page.)

(See figure on previous page.)

Fig. 5 ACT001 suppresses the activation of STING→NF-κB pathway in microglia. **(A-C)** Analysis of RNA-seq of sorted single live Tmem119$^+$ cells in CNS lesions from EAE-control and ACT001-treated mice at the peak of EAE ($n=3$ per group). **(A)** Heatmap displays the expression of all differentiation (DE) genes in SCs microglia based on the RNA-seq data. **(B)** Volcano plot depicts DE genes in SCs microglia. Colored dots represent significant DE genes. DE genes were identified using DEseq2, applying the Wald test with Benjamini-Hochberg correction to determine the false discovery rate (FDR < 0.01). **(D)** Sorted single live Tmem119$^+$ cells in CNS lesions were isolated and analyzed for expression of genes related to STING→NF-κB induced microglia activation ($n=6$ per group). **(E-F)** Immunofluorescence analysis of p-STING (green) **(E)** and p-p65 (green) **(F)** levels in Iba1$^+$(red) microglia within SCs tissue. DAPI (blue) was used as a nuclear marker. Scale bar represents 50 μm. **(G)** Phosphorylation of key proteins in STING→NF-κB pathway in the SCs tissue at Day 0, Day 10, Day 20 and Day 30 following EAE induction. **(H-I)** Phosphorylation of key proteins in STING→NF-κB pathway in primary microglia stimulated by LPS, 2'3'-cGAMP, and HSV-1, and the effects of ACT001. The values in the graph represent the normalized ratio of phosphorylated to total proteins. Statistics were calculated using the unpaired sample *t*-test **(D)** and one-way ANOVA with Tukey's correction **(E, F)**. Error bars denote the mean ± SEM, ns = not significant, $^*p<0.05$, $^{**}p<0.01$ and $^{***}p<0.001$

microglia did not express CD4 (Fig. 4E, H), whereas a subset of doublets co-expressed CD4 and Tmem119 (Fig. 4F, H), capturing the interacting microglia-CD4$^+$ T cells in vivo within EAE lesions. Additionally, the microglia interacting with CD4$^+$ T cells exhibited significantly higher levels of MHC-II compared to the microglia in single-cell state (Fig. 4E-H), which provided evidence supporting the critical role of MHC-II in mediating microglia-CD4$^+$ T cell interactions. Furthermore, ACT001 reduced MHC-II expression on the microglia (Fig. 4E-H) and decreased the interactions between microglia and CD4$^+$ T cells (Fig. 4F, G, I).

ACT001 targets STING→NF-κB pathway to inhibit microglial activation

To further investigate the molecular basis of the regulation of microglia by ACT001 in the effector phase of EAE, we performed RNA-seq analysis on Tmem119$^+$ microglia isolated from the SCs of control or ACT001-treated EAE mice (Fig. S6A). It turned out that ACT001 significantly downregulated genes associated with microglial activation, such as *Il1b*, *Il6*, *Tnf* and *Csf2*, and increased the expression of genes related to inflammation suppression (Fig. 5A, B). Additionally, pathways associated with inflammatory/active microglia (TNF, JAK-STAT and NF-κB pathways) and Th17 differentiation were enriched as downregulated upon ACT001 treatment (Fig. 5C and Fig. S6B). The findings were confirmed by qPCR, as the mRNA expressions by these microglia of *Il6*, *Ccl5*, *Il1b*, *Tnf*, and *Ccl20*, all of which were transcriptional targets of NF-κB, decreased by ACT001. The RNA-seq analysis indicated as well downregulation of pathways related to cytosolic DNA sensing and HSV-1 (a double-stranded DNA virus) infection after ACT001 treatment (Fig. 5C and Fig. S6B), suggesting that ACT001 may exert its effects by modulating cytosolic DNA sensor related pathways [37–39]. cGAS is one of the most important cytosolic DNA sensors [40]. In the CNS, DNA from damaged cells engulfed by microglia or the leakage of mtDNA in aging microglia could active cGAS-STING pathway, which subsequently triggers microglial activation in various neuroinflammatory diseases, including EAE/MS [41–44]. Therefore, we hypothesized that the hyperactive cGAS-STING in the microglia of EAE mice led to the activation of the downstream NF-κB signaling pathway [45–47], which further stimulated the activation of microglia and the subsequent antigen presentation to Th17 cells; ACT001 inhibited STING→NF-κB pathway to reduce the activation of microglia and to suppress the activation of Th17.

To test the hypothesis, we first assess the role of the STING→NF-κB pathway in microglial activation during EAE. At the peak of EAE, significant phosphorylation of both STING and NF-κB (p65) and the nuclear translocation of phosphorylated p65 were observed in Iba1$^+$ microglia from CNS tissues of EAE mice (Fig. 5E, F and Fig. S7). Additionally, the phosphorylation of STING, IKKβ, IκBα and p65, indicating the activation of the STING→NF-κB pathway, increased along with the progression of EAE from immunization (day 0), onset (day 10) to peak (day 20) (Fig. 5G), suggesting a crucial role of the STING→NF-κB pathway in the pathogenesis of EAE. ACT001 reduced the nuclear translocation of p65 as well as the phosphorylation of STING and p65 (Fig. 5E, F and Fig. S7) in microglia of the EAE mice. To further confirm that ACT001 suppressed STING→NF-κB pathway, mouse primary microglia were stimulated with 2'3'-cGAMP, HSV-1 (both are canonical ligands of cGAS-STING) or LPS, and treated with ACT001. All of the three stimulators led to increased mRNA expression of the inflammatory effector genes in microglia, including pro-inflammatory cytokines (*Il1b*, *Il6* and *Tnf*), microglial activation markers (*B2m*, *Ciita* and *Cd80*) and inflammatory chemokines (*Ccl3*, *Ccl4*, *Ccl5*, *Cxcl9*, *Cxcl10*, *Cxcl11* and *Cxcl20*) (Fig. S8 and S9), with 2'3'-cGAMP and HSV-1, canonical stimulators of cGAS-STING, being at least as potent as LPS, the gold-standard stimulator of monocytes and macrophages. Furthermore, ACT001 decreased the phosphorylation of STING, IKKβ, IκBα and p65 in a dosage-dependent manner in both 2'3'-cGAMP and HSV-1 stimulated groups (Fig. 5H, I); it reduced the mRNA expression of the inflammatory effector genes as well in these cells (Fig. S8 and S9). However, in the primary microglia stimulated by LPS, ACT001 had much weaker effect on the phosphorylation of STING, IKKβ, IκBα and p65 (Fig. 5H, I), or on the elevated

mRNA expression of the inflammatory effector genes (Fig. S8 and S9). These findings collectively revealed that STING→NF-κB pathway was active in the microglia of EAE mice, and that ACT001 was able to effectively suppress the activity of STING→NF-κB pathway induced by 2'3'-cGAMP and HSV-1, whereas its inhibitory effect on the LPS-induced, non-STING-dependent NF-κB pathway was less pronounced.

To determine whether ACT001 exerted its therapeutic effects for EAE by suppression of effector pathways of STING in vivo, we induced EAE in both wild-type (WT) and *Sting1*$^{-/-}$ mice. The *Sting1*$^{-/-}$ mice had much milder diseases, with significantly lower EAE clinical scores, reduced infiltration of immune cells in the SCs and a marked downregulation of the Th17 effector program compared to the WT mice (Fig. 6A-H), suggesting STING was an important contributor for EAE. Additionally, ACT001 did not exhibit any additional therapeutic effects on EAE in *Sting1*$^{-/-}$ mice (Fig. 6A-H), which confirmed that the therapeutic effects of ACT001 in EAE were likely primarily mediated via STING.

Based on the results we had so far, we concluded that ACT001 inhibited STING, which subsequently decreased the activation of the STING→NF-κB pathway, thereby inhibiting microglial activation. Since microglia serve as the primary antigen-presenting cells in the CNS, the suppression of microglial activity might indirectly contribute to the reduced Th17 cell activation, which would explain

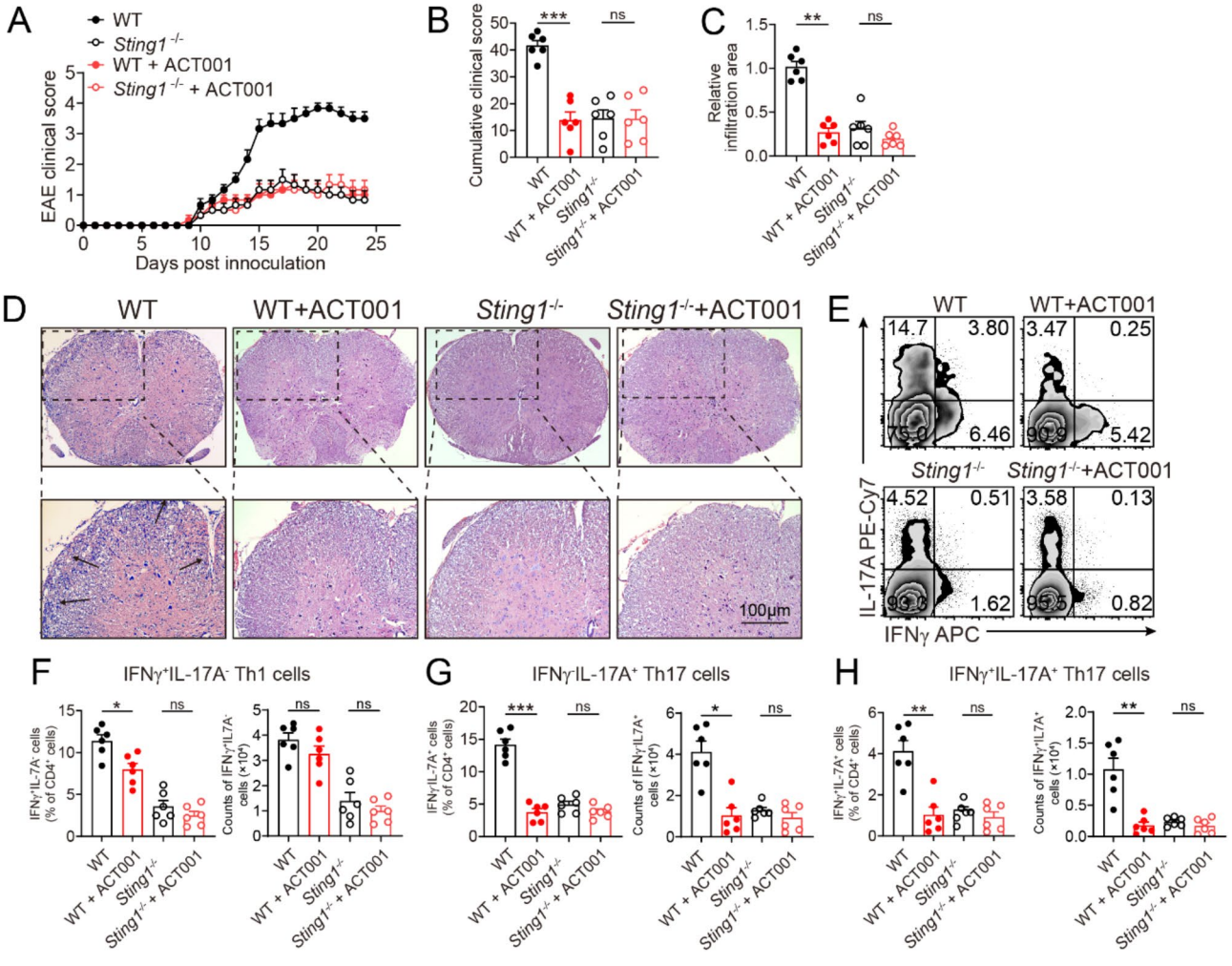

Fig. 6 STING mediates the therapeutic effect of ACT001 on EAE. **(A-B)** The severity of EAE in wild-type (WT) and *Sting1*$^{-/-}$ mice receiving ACT001 treatments ($n=6$ per group). **(A)** Mean daily disease score of symptomatic mice. **(B)** Cumulative clinical score of EAE symptomatic mice. **(C-G)** Infiltration of inflammatory cells in the SCs at the peak of EAE ($n=6$ per group). **(C)** Quantitative analysis of inflammatory cell infiltration areas in transverse sections of the SCs tissue in **(D)**. **(D)** Representative H&E staining pictures. **(E)** Representative flow cytometry analysis of SCs-infiltrating Th1 and Th17 cells. **(F-H)** Statistical analysis of the frequencies and absolute numbers of Th1 **(F)**, IFNγ$^-$ Th17 **(G)**, IFNγ$^+$ Th17 and cells **(H)**. Statistics were calculated using one-way ANOVA with Tukey's correction. Error bars represent the mean ± SEM with ns indicating not significant, *$p<0.05$, **$p<0.01$, and ***$p<0.001$

the discrepancy between the facts that ACT001 inhibited the activation phase of Th17 in vivo but had no effect on Th17 cells alone in vitro. To validate this hypothesis, we conducted further experiments to elucidate the mechanisms underlying the interactions between microglia and Th17 cells.

ACT001 disrupts the microglia-Th17 feed-forward activation loop

ACT001 suppressed the Th17 effector program in the EAE mice without affecting the priming of Th17 cells (Fig. 3 and Fig. S3). It also decreased MHC-II expression on microglia and reduced MHC-II dependent interactions between microglia and $CD4^+$ T cells (Fig. 4E-I). These observations suggested that, in the EAE mice, microglia interacted with EAE-pathogenic Th17 cells as antigen-presenting cells, and active microglia could activate EAE-pathogenic Th17 cells and promote the effector program of the cells.

To support the hypothesis that ACT001 indirectly inhibited the effector program of EAE-pathogenic Th17 cells by suppression of microglia, we conducted co-culture experiments (Fig. S10). Microglia were initially stimulated with 2'3'-cGAMP to activate the STING→NF-κB pathway, which resulted in the increased expression of activation markers, such as iNOS, and decreased expression of homeostatic markers like CD206, indicating an active state of the microglia (Fig. 7A, B) [32]. When ACT001 was included, the elevated iNOS induced by 2'3'-cGAMP decreased significantly, while the suppressed expression of CD206 increased back to the level similar to that of the PBS-control (Fig. 7A, B). At mRNA level, ACT001 suppressed the elevated expression of *Nos2* and *Tnf* induced by 2'3'-cGAMP, while preserved the expression of *Mrc1* and *Il10* (Fig. 7C) [32, 33]. Therefore, ACT001 effectively inhibited 2'3'-cGAMP-induced activation of microglia.

$CD4^+$ T cells from iLNs of 2D2 mice were co-cultured with microglia pre-treated by ACT001 under Th17-diffferentiation condition to assess the impact of microglia on Th17 cells and to explore the involvement of the STING→NF-κB in microglia-Th17 interaction (Fig. S10) [6, 48]. In this experiment, ACT001 did not affect the percentage of IL-17^+ cells among the $CD4^+$ T cells in the absence of microglia (Fig. 7D, E), consistent with the previous results (Fig. S3). Among the $CD4^+$ T cells co-cultured with homeostatic microglia that were not stimulated by 2'3'-cGAMP, the portion of IL-17^+ cells was smaller; whereas active microglia, stimulated with 2'3'-cGAMP, increased the percentage of IL-17 A^+ cells (Fig. 7D, E). With ACT001 pretreatment, microglia suppressed the IL-17^+ population in the $CD4^+$ T cells, regardless of 2'3'-cGAMP (Fig. 7D, E). The mRNA expression of *Il17a* and *Rorc*, the major genes of the Th17 effector program, in the $CD4^+$ T cells confirmed that microglia activated by 2'3'-cGAMP promoted Th17 effector program, whereas ACT001 inhibited this effect of microglia.

Next, we investigated whether Th17 cells promoted microglial activation by the co-culture experiment. Firstly, it turned out that the mRNA expression of *Ciita* and *Il1b*, markers and effectors of microglial activation, increased dramatically by stimulation with 2'3'-cGAMP (Fig. 7G); co-culture with Th17 cells further increased the expression of both genes, indicating that Th17 cells were able to promote the activation of microglia. Interestingly, the activation of microglia by Th17 was dependent as well on the duration of 2'3'-cGAMP stimulations, as the microglia stimulated by 2'3'-cGAMP for 16 h expressed more *Ciita* and *Il1b* than the cells stimulated for 8 h (Fig. 7G). Thus, it is possible that the microglia in EAE lesions are activated by a two-step activation: the first step primes microglia, potentially mediated by STING→NF-κB pathway; and in the second step the microglia are activated by Th17 cells. Therefore, the findings from co-culture experiments suggested that microglia are capable of activating Th17, and Th17 cells could, in turn, promote microglial activation, demonstrating the existence of a feed-forward activation loop between microglia and Th17 cells.

In summary, our results demonstrate that the STING→NF-κB pathway is involved in the pathogenesis of EAE by mediating microglial activation and facilitating the formation of a microglia-Th17 feed-forward activation loop to reinforce and stabilize the effector function of Th17 in EAE. ACT001 ameliorates the autoimmune inflammations in EAE by inhibiting the STING→NF-κB pathway in microglia, thereby disrupting the feed-forward activation loop between microglia and Th17 cells.

Discussion

Studies on T cell activation across various contexts, including infections, autoimmune diseases, and tumors have significantly enhanced our understanding of the activation mechanisms of T cell mediated immune responses as well as the pathogenesis of the diseases [8, 49, 50]. In EAE, the mouse model of the immune aspects of CNS demyelinating disease, researchers have increasingly recognized the activation of pathogenic Th17 cells as a two-step, continuous process involving an initial priming phase in the draining lymph nodes, and followed by an activation phase, or effector differentiation, at neuroinflammatory sites in the CNS [6, 8, 21]. This "two-step" model of Th17 activation highlights the critical role of the CNS environment in intensifying the autoimmune neuroinflammation through interactions between Th17 and local APCs, particularly microglia that are the tissue resident macrophages and most abundant APCs in the

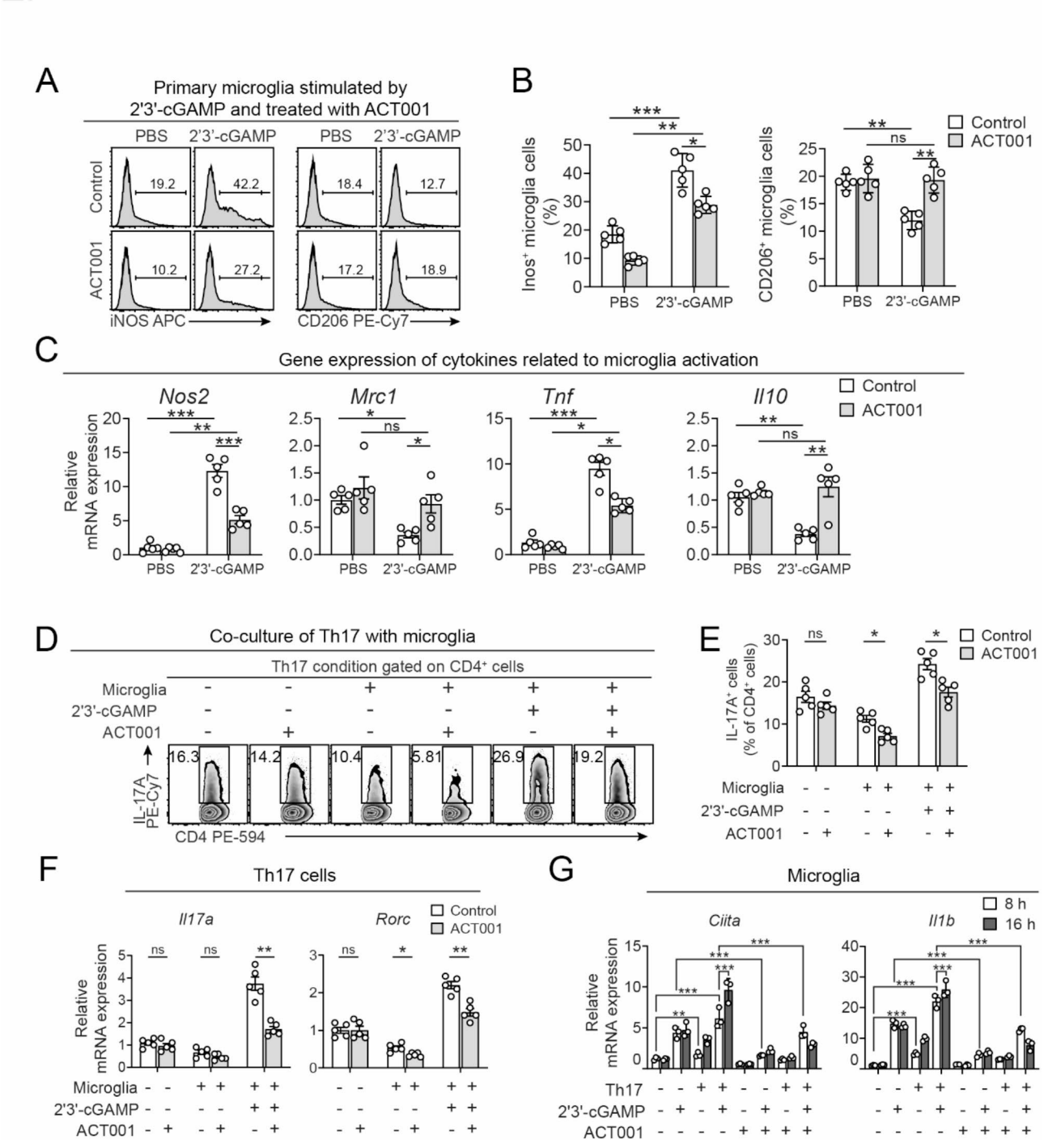

Fig. 7 ACT001 disrupts the feed-forward activation loop between microglia and Th17 cells in vitro. **(A-B)** Flow cytometry analysis of the inhibitory effect of ACT001 on 2′3′-cGAMP-induced activation of primary microglia ($n = 5$ per group). **(A)** Representative flow cytometry results demonstrating the effect of ACT001 on iNOS and CD206 expression in 2′3′-cGAMP-activated primary microglia. **(B)** Statistical analysis of the frequencies of iNOS$^+$ and CD206$^+$ microglia in **(A)**. **(C)** Primary microglia were treated as described in **(A)** and analyzed for mRNA expression of cytokines related to microglial activation ($n = 6$ per group). **(D-G)** In vitro co-culture experiments were conducted to evaluate the activation of microglia and Th17 cells following co-culture. **(D)** Representative flow cytometry analysis of IL-17 A in the Th17 cells following co-cultured with microglia treated with 2′3′-cGAMP and ACT001. **(E)** Statistical analysis of the frequencies and absolute numbers of Th17 cells in **(D)**. **(F)** Normalized mRNA expressions of *Il17a* and *Rorc* in the Th17 cells following co-culture as described in **(D)** ($n = 5$ per group). **(G)** Normalized mRNA expressions of *Ciita* and *Il1b* in microglia after 8–16 h of co-culture with Th17 cells as described in **(D)**. ($n = 5$ per group). Statistics were calculated using one-way ANOVA with Tukey's correction. Error bars represent the mean ± SEM with ns indicating not significant, $^*p < 0.05$, $^{**}p < 0.01$, and $^{***}p < 0.001$

CNS [4, 6, 9]. In this study, we provided more evidence for the model. By using an in vitro microglia-Th17 co-culture system, we dissected the interactions between the two types of cells that are of importance in the pathogenesis of EAE/MS. The findings reveal that the interactions are bi-directional, as active microglia activate Th17 and Th17 in turn enhance the activation of microglia. Thus, a feed-forward loop formed to reinforce and stabilize both the active state of microglia and the effector program of pathogenic Th17 cells, contributing to the pathogenesis of the disease. The microglia-$CD4^+$ T cell interactions were visualized as two-cell units in tissue samples from the CNS of EAE mice. It was clear that the numbers of the two-cell units correlated with the severity of EAE. Furthermore, the microglia in the two-cell units expressed much higher levels of CD45 and MHC-II than the single microglia, indicating that the cells were in active state. Therefore, we propose that the interactions between microglia and Th17 cells form a feed-forward activation loop, which is the immunopathogenic basis of EAE/MS.

Several studies have indicated that the interaction between APCs and Th17 plays a critical role in sustaining CNS inflammation. Although these researches have highlighted the importance of the interaction, the direct evidence remains limited, and the underlying mechanisms are not yet fully understood [6, 51–55]. Our study bridges this gap by demonstrating that (i) active microglia, as professional APCs, sustain Th17 activation in EAE; (ii) elevated MHC-II expression on the active microglia is essential for their prolonged interaction with Th17 cells, further exacerbating neuroinflammation; (iii) the initiator of microglial activation may be STING→NF-κB signaling pathway; and (iv) once activated, the active state of microglia is stabilized by Th17 cells. The activation of both microglia and Th17 cells establishes a feed-forward activation loop to amplify local neuroinflammation.

This study was originally aimed to investigate the mechanism by which ACT001 ameliorates EAE. The schema was to administrate ACT001 to the mice at different stages of EAE, namely the induction phase and the effector phase, to pinpoint its mode of action. The results demonstrated that ACT001 exerted the therapeutic effect specifically during the effector phase of EAE without observed impact in the induction phase. At cellular level, ACT001 selectively targets the activation of Th17 cells in the CNS rather than their initial priming phase in iLNs. Treatment with ACT001 during the effector phase reduced both the infiltration of Th17 cells in the EAE lesions and suppressed the expression of key pathogenic inflammatory cytokines *Csf2* and *Ifng*, resulting a much milder disease. The findings as well as that fact that ACT001 has been approved by the US FDA as an orphan drug for glioblastomas suggested the potential application of ACT001 as a therapeutic agent for autoimmune neuroinflammatory diseases [10, 14, 15].

A surprising finding from the dissection of the inhibitory effects of ACT001 on Th17 in the EAE lesions was that the cellular targets of ACT001 were not the pathogenic Th17 cells as we originally speculated based on the phenotypes of the EAE mice; instead, ACT001 mediated its therapeutic effects through the suppression of microglia. Specifically, ACT001 reduced the proportion of active microglia ($CD11b^+CD45^{Hi}$) and maintained a higher proportion of homeostatic microglia ($CD11b^+CD45^{dim}$) in the EAE lesions. Accordingly, we observed the reduced expression of MHC-II and iNOS in microglia from ACT001-treated mice. At molecular level, ACT001 suppressed STING and the downstream NF-κB pathway. The suppression of microglia disrupted the microglia-Th17 feed-forward activation loop in EAE, which reduced the autoimmune neuroinflammations of the disease.

STING is a major mediator for autoimmune inflammation, but the outcomes of targeting STING in EAE/MS are complex. Several studies [56–59] including the current one, have found that inhibiting STING suppresses neuroinflammation; however, some literatures show that agonistically activating the STING-dependent Type I interferon response suppresses the inflammation [60, 61]. We speculate that the discrepancies could be due to the fact that there are two major effector pathways downstream of STING activation. One of the pathways is IRF3-Type I interferon which improves the outcome of EAE and some MS patients. The other downstream effector pathway of STING is NF-κB that orchestrates the genetic program for inflammation [62, 63]. We have observed that ACT001 suppresses STING→NF-κB effector pathway with little impact on the production of IFNβ, which may explain the distinct outcome of EAE treated with STING antagonist ACT001 in contrast to the studies of STING being targeted agonistically so as to improve EAE outcomes.

Our study provides insights into the role of microglia-Th17 interaction in the pathogenesis of EAE, but two limitations should be considered. First, the expression of TMEM119 is known to decrease in active microglia, which may affect the analysis and interpretation [36]. We tried to address this concern by gating on CD11b/CD45 prior to evaluating TMEM119 expression (Fig. S11A). Although $CD11b^+CD45^{Hi}$ microglia showed decreased TMEM119 expression compared to homeostatic $CD11b^+CD45^{dim}$ microglia, we have found that their TMEM119 expression was not completely absent (Fig. S11A, purple populations), and they could still be distinguished from TMEM119-negative cells. To further address this concern, we compared this gating strategy with the strategy used in Fig. 4, and found no significant difference between them (Fig. S11B). As for another

limitation, while we observed that ACT001 targets microglia to suppress Th17 in the effector phase of EAE, our study did not directly investigate the role of microglial MHC-II in Th17 activation and EAE progression. The results do not exclude the possibility of a redundant role of MHC-II [64, 65].

To summarize, our results demonstrate that ACT001 ameliorates EAE by targeting the STING→NF-κB pathway in microglia, effectively disrupting the microglia-Th17 feed-forward activation loop. These findings provide immunopathologic rationales for future study of the application of ACT001 to treat neuroinflammatory diseases, including multiple sclerosis.

Supplementary Information

The online version contains supplementary material available at https://doi.org/10.1186/s12974-025-03427-1.

Supplementary Material 1

Supplementary Material 2

Supplementary Material 3

Acknowledgements
The authors thank members of our research group, especially Dr. Jian Zheng, Guangyue Fan, Dr. Zhenyi Xue and Dr. Jie Yin for helpful discussions and for sharing reagents before publication.

Author contributions
J.X. designed and performed research, analyzed data, and wrote the manuscript; Z.M., Y.L., Z.N. and Y.L. performed research and analyzed data; Z.Y. and Y.Z designed research and analyzed data; L.L. designed research, analyzed data, and wrote the manuscript.

Funding
This work was supported by the National Natural Science Foundation of China (32270970), the Tianjin Municipal Science and Technology Program (22JCYBJC00440, 23JCZXJC00360), and the Chinese Academy of Medical Sciences Innovation Fund for Medical Sciences grant (2023-I2M-2-007).

Data availability
RNA-seq data that support the findings of this study have been deposited at https://datadryad.org, with the digital ID DOI: 10.5061/dryad.98sf7m0tm.

Declarations

Ethics approval and consent to participate
Not applicable.

Consent for publication
Not applicable.

Competing interests
The authors declare no competing interests.

Received: 31 January 2025 / Accepted: 24 March 2025
Published online: 24 April 2025

References

1. Attfield KE, Jensen LT, Kaufmann M, Friese MA, Fugger L. The immunology of multiple sclerosis. Nat Rev Immunol. 2022;22:734–50.
2. Laaker C, Hsu M, Fabry Z, Miller SD, Karpus WJ. Experimental autoimmune encephalomyelitis in the mouse. Curr Protocols. 2021;1:e300.
3. Baxter AG. The origin and application of experimental autoimmune encephalomyelitis. Nat Rev Immunol. 2007;7:904–12.
4. Distéfano-Gagné F, Bitarafan S, Lacroix S, Gosselin D. Roles and regulation of microglia activity in multiple sclerosis: insights from animal models. Nat Rev Neurosci. 2023;24:397–415.
5. Constantinescu CS, Farooqi N, O'Brien K, Gran B. Experimental autoimmune encephalomyelitis (EAE) as a model for multiple sclerosis (MS). Br J Pharmacol. 2011;164:1079–106.
6. Kedmi R, Littman DR. Antigen-presenting cells as specialized drivers of intestinal T cell functions. Immunity. 2024;57:2269–79.
7. Hall JA, Pokrovskii M, Kroehling L, Kim B-R, Kim SY, Wu L, et al. Transcription factor RORα enforces stability of the Th17 cell effector program by binding to a *Rorc cis*-regulatory element. Immunity. 2022;55:2027–e20439.
8. Kopp EB, Agaronyan K, Licona-Limón I, Nish SA, Medzhitov R. Modes of type 2 immune response initiation. Immunity. 2023;56:687–94.
9. Mader MM-D, Napole A, Atkins M, Scavetti A, Shibuya Y, Foltz A, et al. Myeloid cell replacement is neuroprotective in chronic experimental autoimmune encephalomyelitis. Nat Neurosci. 2024;27:901–12.
10. Xi X, Liu N, Wang Q, Chu Y, Yin Z, Ding Y, et al. ACT001, a novel PAI-1 inhibitor, exerts synergistic effects in combination with cisplatin by inhibiting PI3K/AKT pathway in glioma. Cell Death Dis. 2019;10:757.
11. Zhang Q, Lu Y, Ding Y, Zhai J, Ji Q, Ma W, et al. Guaianolide sesquiterpene lactones, a source to discover agents that selectively inhibit acute myelogenous leukemia stem and progenitor cells. J Med Chem. 2012;55:8757–69.
12. Peng Z, Lv X, Wang X, Shang T, Chang J, Salahdiin K, et al. ACT001 improved cardiovascular function in septic mice by inhibiting the production of Pro-inflammatory cytokines and the expression of JAK-STAT signaling pathway. Front Pharmacol. 2023;14:1265177.
13. Lickliter JD, Jennens R, Lemech CR, Kichenadasse G, Cai D, Su SY-C. Phase 1 dose-escalation study of ACT001 in patients with recurrent glioblastoma and other advanced solid tumors. JCO. 2021;39:2037–2037.
14. Hou Y, Sun B, Liu W, Yu B, Shi Q, Luo F, et al. Targeting of glioma stem-like cells with a parthenolide derivative ACT001 through Inhibition of AEBP1/PI3K/AKT signaling. Theranostics. 2021;11:555–66.
15. Tong L, Li J, Li Q, Wang X, Medikonda R, Zhao T, et al. ACT001 reduces the expression of PD-L1 by inhibiting the phosphorylation of STAT3 in glioblastoma. Theranostics. 2020;10:5943–56.
16. Cai L, Gong Q, Qi L, Xu T, Suo Q, Li X, et al. ACT001 attenuates microglia-mediated neuroinflammation after traumatic brain injury via inhibiting AKT/NFκB/NLRP3 pathway. Cell Commun Signal. 2022;20:56.
17. Laaker C, Hsu M, Fabry Z, Miller SD, Karpus WJ. Experimental autoimmune encephalomyelitis in the mouse. Curr Protoc. 2021;1:e300.
18. Rangachari M, Zhu C, Sakuishi K, Xiao S, Karman J, Chen A, et al. Bat3 promotes T cell responses and autoimmunity by repressing Tim-3–mediated cell death and exhaustion. Nat Med. 2012;18:1394–400.
19. Jäger A, Dardalhon V, Sobel RA, Bettelli E, Kuchroo VK. Th1, Th17, and Th9 effector cells induce experimental autoimmune encephalomyelitis with different pathological phenotypes. J Immunol. 2009;183:7169–77.
20. Zhou L, Chong MMW, Littman DR. Plasticity of CD4$^+$ T cell lineage differentiation. Immunity. 2009;30:646–55.
21. Schnell A, Littman DR, Kuchroo VK. T_H17 cell heterogeneity and its role in tissue inflammation. Nat Immunol. 2023;24:19–29.
22. Lee Y, Awasthi A, Yosef N, Quintana FJ, Xiao S, Peters A, et al. Induction and molecular signature of pathogenic T_H17 cells. Nat Immunol. 2012;13:991–9.
23. Gao Y, Wang Y, Chauss D, Villarino AV, Link VM, Nagashima H, et al. Transcription factor EGR2 controls homing and pathogenicity of T_H17 cells in the central nervous system. Nat Immunol. 2023;24:1331–44.
24. Mangani D, Subramanian A, Huang L, Cheng H, Krovi SH, Wu Y, et al. Transcription factor TCF1 binds to RORγt and orchestrates a regulatory network that determines homeostatic Th17 cell state. Immunity. 2024;57:2565–e25826.
25. Thakore PI, Schnell A, Huang L, Zhao M, Hou Y, Christian E, et al. BACH2 regulates diversification of regulatory and Proinflammatory chromatin States in T_H17 cells. Nat Immunol. 2024;25:1395–410.
26. Marusic S, Leach MW, Pelker JW, Azoitei ML, Uozumi N, Cui J, et al. Cytosolic phospholipase A2α–deficient mice are resistant to experimental autoimmune encephalomyelitis. J Exp Med. 2005;202:841–51.
27. Thakker P, Leach MW, Kuang W, Benoit SE, Leonard JP, Marusic S. IL-23 is critical in the induction but not in the effector phase of experimental autoimmune encephalomyelitis. J Immunol. 2007;178:2589–98.

28. Lee J-Y, Hall JA, Kroehling L, Wu L, Najar T, Nguyen HH, et al. Serum amyloid A proteins induce pathogenic Th17 cells and promote inflammatory disease. Cell. 2020;180:79–e9116.
29. Hou Y, Sun L, LaFleur MW, Huang L, Lambden C, Thakore PI, et al. Neuropeptide signalling orchestrates T cell differentiation. Nature. 2024;635:444–52.
30. Iwasaki A, Medzhitov R. Control of adaptive immunity by the innate immune system. Nat Immunol. 2015;16:343–53.
31. Voet S, Prinz M, Van Loo G. Microglia in central nervous system inflammation and multiple sclerosis pathology. Trends Mol Med. 2019;25:112–23.
32. Li Q, Barres BA. Microglia and macrophages in brain homeostasis and disease. Nat Rev Immunol. 2018;18:225–42.
33. De Vlaminck K, Van Hove H, Kancheva D, Scheyltjens I, Pombo Antunes AR, Bastos J, et al. Differential plasticity and fate of brain-resident and recruited macrophages during the onset and resolution of neuroinflammation. Immunity. 2022;55:2085–e21029.
34. Haimon Z, Frumer GR, Kim J-S, Trzebanski S, Haffner-Krausz R, Ben-Dor S, et al. Cognate microglia–T cell interactions shape the functional regulatory T cell pool in experimental autoimmune encephalomyelitis pathology. Nat Immunol. 2022;23:1749–62.
35. Jie Z, Ko C-J, Wang H, Xie X, Li Y, Gu M, et al. Microglia promote autoimmune inflammation via the noncanonical NF-κB pathway. Sci Adv. 2021;7:eabh0609.
36. Paolicelli RC, Sierra A, Stevens B, Tremblay M-E, Aguzzi A, Ajami B, et al. Microglia States and nomenclature: A field at its crossroads. Neuron. 2022;110:3458–83.
37. Ablasser A, Hur S. Regulation of cGAS- and RLR-mediated immunity to nucleic acids. Nat Immunol. 2020;21:17–29.
38. Roers A, Hiller B, Hornung V. Recognition of endogenous nucleic acids by the innate immune system. Immunity. 2016;44:739–54.
39. Paludan SR, Bowie AG. Immune sensing of DNA. Immunity. 2013;38:870–80.
40. Ablasser A, Chen ZJ. cGAS in action: expanding roles in immunity and inflammation. Science. 2019;363:eaat8657.
41. Ding R, Li H, Liu Y, Ou W, Zhang X, Chai H, et al. Activating cGAS–STING axis contributes to neuroinflammation in CVST mouse model and induces inflammasome activation and microglia pyroptosis. J Neuroinflamm. 2022;19:137.
42. Hou Y, Wei Y, Lautrup S, Yang B, Wang Y, Cordonnier S, et al. NAD^+ supplementation reduces neuroinflammation and cell senescence in a Transgenic mouse model of Alzheimer's disease via cGAS-STING. Proc Natl Acad Sci U S A. 2021;118:e2011226118.
43. Jin M, Shiwaku H, Tanaka H, Obita T, Ohuchi S, Yoshioka Y, et al. Tau activates microglia via the PQBP1-cGAS-STING pathway to promote brain inflammation. Nat Commun. 2021;12:6565.
44. Gulen MF, Samson N, Keller A, Schwabenland M, Liu C, Glück S, et al. cGAS-STING drives ageing-related inflammation and neurodegeneration. Nature. 2023;620:374–80.
45. Zhang X, Bai X-C, Chen ZJ. Structures and mechanisms in the cGAS-STING innate immunity pathway. Immunity. 2020;53:43–53.
46. Hopfner K-P, Hornung V. Molecular mechanisms and cellular functions of cGAS-STING signalling. Nat Rev Mol Cell Biol. 2020;21:501–21.
47. Li T, Yum S, Li M, Chen X, Zuo X, Chen ZJ. TBK1 recruitment to STING mediates autoinflammatory arthritis caused by defective DNA clearance. J Exp Med. 2022;219:e20211539.
48. Bettelli E, Pagany M, Weiner HL, Linington C, Sobel RA, Kuchroo VK. Myelin oligodendrocyte Glycoprotein–specific T cell receptor Transgenic mice develop spontaneous autoimmune optic neuritis. J Exp Med. 2003;197:1073–81.
49. Flintoft L. Throwing LIGHT on tumour rejection. Nat Rev Cancer. 2004;4:89–89.
50. Shakiba M, Zumbo P, Espinosa-Carrasco G, Menocal L, Dündar F, Carson SE, et al. TCR signal strength defines distinct mechanisms of T cell dysfunction and cancer evasion. J Exp Med. 2022;219:e20201966.
51. Schetters STT, Gomez-Nicola D, Garcia-Vallejo JJ, Van Kooyk Y, Neuroinflammation. Microglia and T cells get ready to Tango. Front Immunol. 2017;8:1905.
52. Grigg JB, Shanmugavadivu A, Regen T, Parkhurst CN, Ahmed A, Joseph AM, et al. Antigen-presenting innate lymphoid cells orchestrate neuroinflammation. Nature. 2021;600:707–12.
53. Mundt S, Mrdjen D, Utz SG, Greter M, Schreiner B, Becher B. Conventional DCs sample and present Myelin antigens in the healthy CNS and allow parenchymal T cell entry to initiate neuroinflammation. Sci Immunol. 2019;4:eaau8380.
54. Pishesha N, Harmand TJ, Ploegh HL. A guide to antigen processing and presentation. Nat Rev Immunol. 2022;22:751–64.
55. Abramson J, Dobeš J, Lyu M, Sonnenberg GF. The emerging family of $ROR\gamma t^+$ antigen-presenting cells. Nat Rev Immunol. 2024;24:64–77.
56. Quan S, Fu X, Cai H, Ren Z, Xu Y, Jia L. The neuroimmune nexus: unraveling the role of the mtDNA-cGAS-STING signal pathway in Alzheimer's disease. Mol Neurodegeneration. 2025;20:25.
57. Woo MS, Mayer C, Binkle-Ladisch L, Sonner JK, Rosenkranz SC, Shaposhnykov A, et al. STING orchestrates the neuronal inflammatory stress response in multiple sclerosis. Cell. 2024;187:4043–e406030.
58. Houston S. Putting the STING in MS. Nat Immunol. 2024;25:1309–1309.
59. Verma SC, Enée E, Manasse K, Rebhi F, Penc A, Romeo-Guitart D, et al. Cathelicidin antimicrobial peptide expression in neutrophils and neurons antagonistically modulates neuroinflammation. J Clin Invest. 2024;135:e184502.
60. Mathur V, Burai R, Vest RT, Bonanno LN, Lehallier B, Zardeneta ME, et al. Activation of the STING-Dependent type I interferon response reduces microglial reactivity and neuroinflammation. Neuron. 2017;96:1290–e13026.
61. Johnson BM, Uchimura T, Gallovic MD, Thamilarasan M, Chou W-C, Gibson SA, et al. STING agonist mitigates experimental autoimmune encephalomyelitis by stimulating type I IFN–Dependent and–Independent Immune-Regulatory pathways. J Immunol. 2021;206:2015–28.
62. Fueyo-González F, McGinty M, Ningoo M, Anderson L, Cantarelli C, Andrea Angeletti, et al. Interferon-β acts directly on T cells to prolong allograft survival by enhancing regulatory T cell induction through Foxp3 acetylation. Immunity. 2022;55:459–e4747.
63. Fryer AL, Abdullah A, Taylor JM, Crack PJ. The complexity of the cGAS-STING pathway in CNS pathologies. Front Neurosci. 2021;15:621501.
64. Jordão MJC, Sankowski R, Brendecke SM, Sagar GL, Locatelli G, Tai Y-H, et al. Single-cell profiling identifies myeloid cell subsets with distinct fates during neuroinflammation. Science. 2019;363:eaat7554.
65. Wolf Y, Shemer A, Levy-Efrati L, Gross M, Kim J-S, Engel A, et al. Microglial MHC class II is dispensable for experimental autoimmune encephalomyelitis and cuprizone-induced demyelination. Eur J Immunol. 2018;48:1308–18.

Publisher's note